*Materials Transactions*, Vol. 60, No. 7 (2019) pp. 1221 to 1229
Special Issue on Severe Plastic Deformation for Nanomaterials with Advanced Functionality



# Metallurgical Alchemy by Ultra-Severe Plastic Deformation via High-Pressure Torsion Process

Kaveh Edalati*

*WPI, International Institute for Carbon-Neutral Energy Research (WPI-I2CNER), Kyushu University, Fukuoka 819-0395, Japan*

Ultra-severe plastic deformation (ultra-SPD) is defined as the SPD processes in which the shear strains over 1,000 are introduced to a work piece. Despite significant activities on various SPD processes, limited studies have been conducted on the behavior of materials at shear strains over 1,000. The main reason for such limited studies is a consensus that the microstructural, mechanical and functional features usually saturate to the steady states at shear strains below 100. However, recent studies using the high-pressure torsion (HPT) method confirmed that significant changes occur at shear strains in the range of 1,000–100,000. Here, some of the main findings reported recently by the application of ultra-SPD are reviewed: appearance of new levels of steady-state microhardness, atomic-scale elemental mixing in the miscible and immiscible systems, formation of new nanostructured phases / intermetallics, achievement of ultrahigh strength / high plasticity / room-temperature superplasticity, and development of advanced superconductors and hydrogen storage materials. [doi:10.2320/matertrans.MF201914]

(Received January 30, 2019; Accepted March 19, 2019; Published May 31, 2019)

***Keywords:*** *severe plastic deformation (SPD), high-pressure torsion (HPT), phase transformations, ultrafine-grained (UFG) materials, functional properties*

## 1. Introduction

Severe plastic deformation (SPD)[1–3] is widely used not only to achieve ultrafine-grained (UFG) materials with advanced structural and functional properties[4–6] but also to control phase transformations[7–9] and conduct mechanical alloying.[10–13] Since the earlier studies using the Bridgman anvils in 1930s,[14,15] many works have shown that the structure and microstructure evolve only at the early stages of straining and all features finally saturate to the steady states at large strains.[16–19]

Despite many studies reported the occurrence of steady state at large strains, the SPD process was conducted mostly by employing normal strains in the range of 10 or shear strains in the range of 100.[1–19] Therefore, the behavior of materials at extremely large strains is not well-understood yet. Although most of the SPD processes are basically applicable under extremely large strains, the high-pressure torsion (HPT) method is technically the most appropriate method to investigate the behavior of materials at extremely large shear strains.[1,20,21] In the HPT method, a thin disc sample is squeezed between two large anvils and shear strain is introduced by rotating the anvils with respect to each other ($\gamma = 2\pi rN/h$; $\gamma$: shear strain; $r$: distance from disc center, $N$: number of turns, $h$: disc thickness).[20,21]

In the studies conducted by the author and his colleagues within the past 10 years, ultra-SPD up to shear strains of 100,000 was imparted in various metallic materials by HPT processing and the evolution of microstructure, phase transformation and properties was investigated. This manuscript briefly reviews the main findings on the application of ultra-SPD to different materials to achieve advanced structural and functional properties. Here, ultra-SPD is defined as the SPD processes in which the shear strains over 1,000 are introduced in the material. The level of 1,000 was selected tentatively because many materials (especially multi-phase ones) start showing some new behaviors over this strain level.

*Corresponding author, E-mail: kaveh.edalati@kyudai.jp

## 2. Application of Ultra-SPD to Various Materials

In the group of author, Ultra-SPD was conducted on various kinds of materials only using the HPT method. For this process, the cylindrical HPT anvils (50 mm diameter and 35 mm height) were fabricated mainly from a tool steel with nitrided surface, but WC - 11% Co composite was occasionally used for processing hard materials. A hole with either 10 or 14 mm diameter, 0.25 mm thickness and 30 μm surface roughness was machined on the surface of each anvil. The samples were either in the form powders or discs with 10 or 14 mm diameter and 0.8 mm thickness. The applied pressure was in the range of 2 to 6 GPa, the rotation speed was 1 rpm and the total number of turns were up to 1,500 turns. Contamination of samples from the anvils was minor, especially for the samples with hardness levels smaller than 400 Hv. In this session, some results achieved by the application of ultra-SPD to different kinds of materials are reviewed.

### 2.1 Pure metals

When pure metals are processed by HPT for $N = 4$–10 turns (i.e. $\gamma = 100$–300), the saturation of grain refinement and hardening occur.[16–18] Although the occurrence of saturation is expected in pure metals due to dynamic recovery,[17,18] dynamic recrystallization,[14,22] grain-boundary rotation[23] and/or grain-boundary migration,[16] there have been limited attempts to examine the occurrence of saturation at shear strains larger than 1,000. The data summarized in Fig. 1 for (a) bcc-Fe,[24] (b) fcc-Ni[24] and (c) hcp-Ti,[25] suggest that some deviations may occur from the saturation levels at $\gamma > 1{,}000$. Deviations in the hardness of HPT-processed Fe from the steady state is also visible in the data reported by Hosokawa *et al.*[26] The exact reason for these deviations, which may not appear for all pure metals, is not

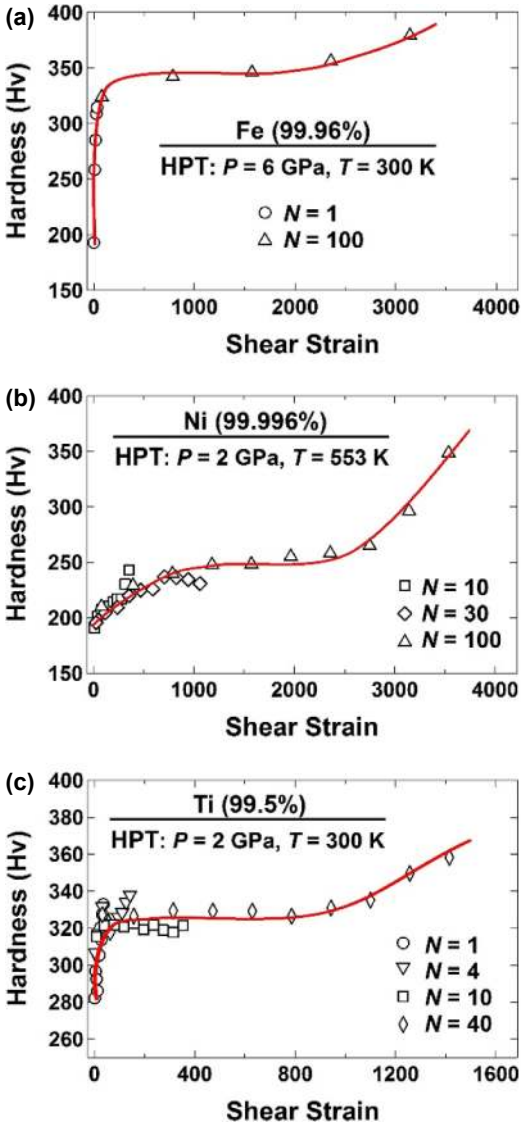


Fig. 1 Deviations from apparent steady-state hardness at very large shear strain. Variations of hardness versus shear strain for (a) bulk Fe,[24] (b) bulk Ni[24] and (c) ball-milled Ti[25] after HPT processing for various turns.

well-understood yet and should be investigated by detailed characterizations in future. However, it can be concluded that a real steady state for some metals should occur at larger shear strains than those are currently accepted.

### 2.2 Miscible systems

Mechanical alloying usually results in the formation of UFG materials which have higher strength compared with the materials synthesized by melting methods. The application of HPT as a mechanical alloying route results not only in the mechanical synthesis but also in the formation of bulk samples, which usually do not require an extra consolidation process.[27,28] When the multi-phase systems with thermodynamic miscibility are subjected to HPT to synthesize a single phase, the magnitude of shear strain required for atomic-scale mixing is always higher than that required for grain refinement in pure metals because of two reasons. First, the phases should be fragmented to reduce the diffusion path. Second, the processing time should be long enough for completion of lattice diffusion.

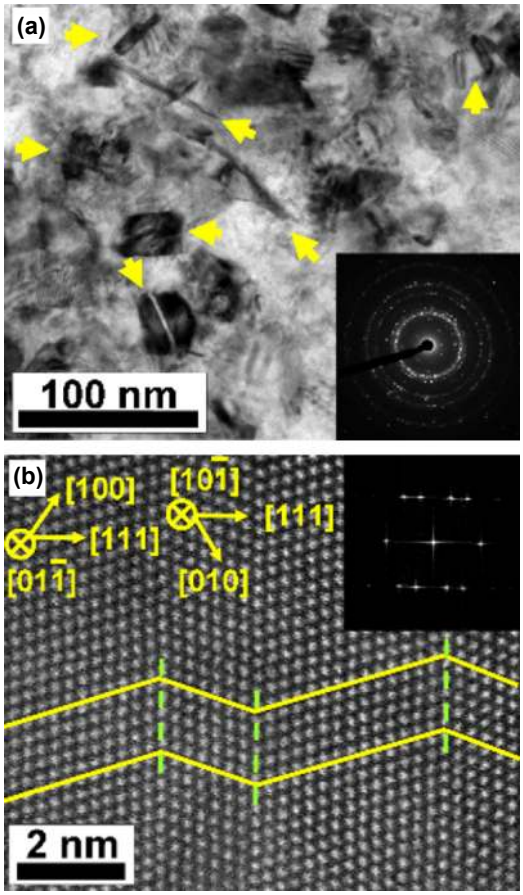


Fig. 2 Nanograined TiAl intermetallic with large fraction of twins synthesized from Ti/Al powders by ultra-SPD. (a) TEM bright-field image and corresponding SAED pattern and (b) lattice image of twins after HPT processing for 50 turns at 573 K followed by annealing at 873 K for 24 h.[32]

We processed powder mixtures in different miscible systems such as Al–Ni,[29–31] Ti–Al,[32,33] Ni–Al–Ti,[33,34] Al–Cu,[35] Fe–Ni[36] and Mg-based systems[37] by the HPT method for up to 120 turns ($\gamma < 5{,}000$). The HPT-processed materials were examined by different techniques such as X-ray diffraction (XRD), scanning electron microscopy (SEM), energy dispersive X-ray spectroscopy (EDS), transmission electron microscopy (TEM), selected area electron diffraction (SAED) analysis, fast Fourier transform (FFT) analysis, scanning transmission electron microscopy (STEM), high-angle annular dark-field (HAADF) imaging and atom probe tomography. It was found that in all cases, mechanical alloying could be conducted successfully. However, since the total imposed strain was limited to a maximum level of 5,000, the single-phase intermetallic phases in some of these systems (especially in those contained soft Al and Mg elements) could be produced only by increasing the processing temperature or by conducting the post-HPT annealing.[29–37]

Figures 2 and 3 show the microstructures of TiAl and $Ni_2AlTi$ intermetallics synthesized from the elemental powders by HPT processing for $N = 50$ turns at 573 K followed by annealing at 873 K for 24 h.[32,34] In both materials, nanograined ordered phases could be successfully synthesized. Although the formation of these nanograined intermetallics with good atomic ordering is not thermody-

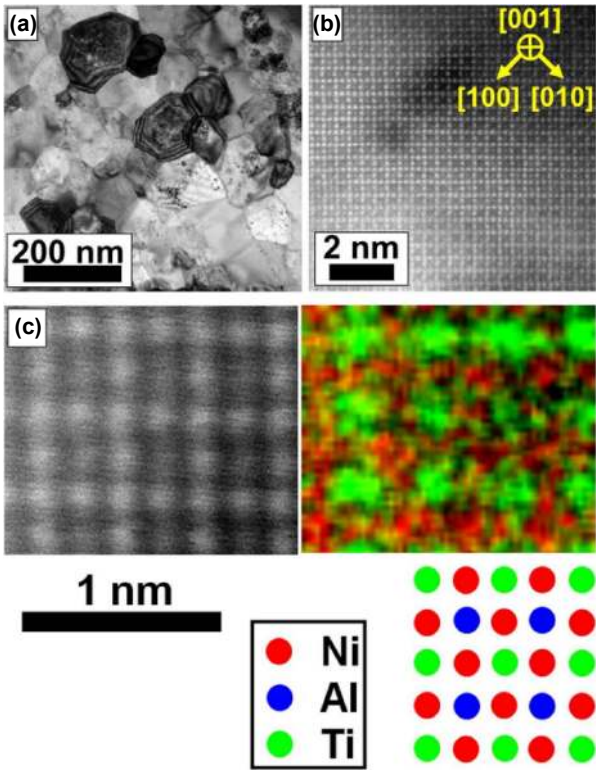


Fig. 3 Ultrafine-grained $Ni_2TiAl$ with $L2_1$ ordering synthesized from elemental powders by ultra-SPD. (a) TEM bright-field image, (b) high-resolution image, and (c) HAADF lattice image and corresponding atomic-scale EDS mapping after HPT processing for 50 turns at 573 K followed by annealing at 873 K for 24 h.[34)]

namically surprising, a simple calculation can show that significant enhancement in the kinetics and lattice diffusion should have occurred during the HPT process. For example, it was shown that the atomic diffusion in the Al–Cu system during the HPT process should be $10^{12}$–$10^{22}$ times higher[35)] than the reported interdiffusion coefficients in this system.[38)] Another good example on the enhancement of kinetics is the formation of $L1_0$ phase in the Fe–Ni system by HPT processing within 100 minutes,[36)] while this phase is formed only in meteorites during long-time astronomical periods.[39)] Such an enhancement in the kinetics is due to the formation of various kinds of lattice defects and particularly due to the formation of vacancies.[40–42)]

### 2.3 Immiscible systems with small heat of mixing

In the immiscible systems, there is no thermodynamic driving force for the atomic-scale mixing at the equilibrium condition because of the positive heat of formation. When the heat of formation in an immiscible system is small such as in Nb–Ti and Ti–V,[43)] the alloys can be successfully synthesized by rapid cooling from the high-temperature regime.[44)] However, when these immiscible systems are severely deformed, the internal energy of the system is changed by lattice defects as well as by dynamic strain effects and accordingly, atomic diffusion and elemental mixing occur.[11,45)] Our studies showed that the formation of metastable phases by mechanical alloying is easier, when the starting elements have hardness levels close to each other and/or when their heat of mixing is not so positive such as in Nb–Ti[46)] and Ti–V.[47)]

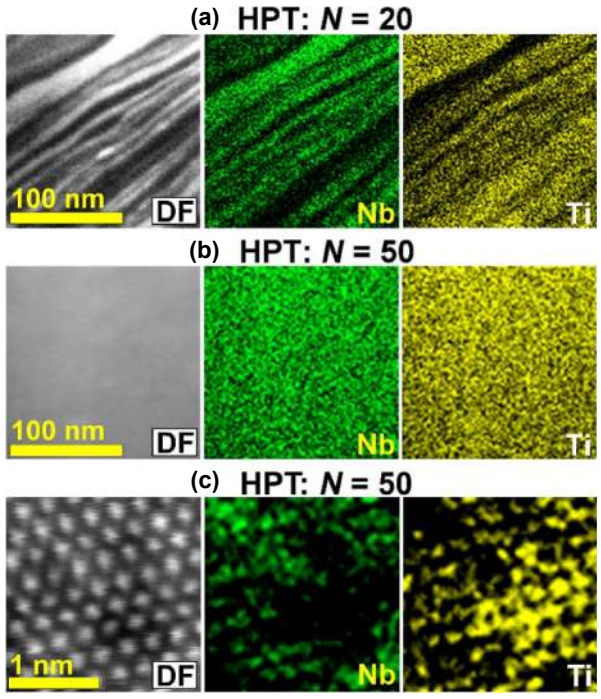


Fig. 4 Synthesis of Nb–Ti alloy from Nb/Ti powders by ultra-SPD. STEM-HAADF and corresponding EDS elemental mappings after HPT processing for (a) 20 and (b, c) 50 turns at room temperature, where (c) shows presence of Ti nano-clusters.[46)]

Figure 4 shows the formation of metastable bcc phases in the Nb–Ti system by HPT processing at room temperature. The elements in the Nb–Ti system were first elongated in the shear direction (Fig. 4(a)) and subsequently mixed by atomic diffusion under large shear strains (Fig. 4(b)).[46)] Despite apparent perfect mixing of the elements after ultra-SPD, which was confirmed by XRD analysis and conventional EDS analysis, detailed atomic-scale elemental mapping confirmed the presence of nano-clusters of Ti with the bcc structure (Fig. 4(c)).[46)] Similar results were achieved for the Ti–V system, in which hcp-Ti and bcc-V were mixed and a metastable bcc phase was formed at ambient temperature.[47)]

### 2.4 Immiscible systems with significant immiscibility

When shear strain is induced in a system with significant immiscibility, the phases are elongated in the shear direction and their thicknesses are reduced. For atomic-scale mixing of immiscible phases, if we assume that the phases are co-deformed ideally, the shear strain should be so high that the thicknesses of sheared phases are reduced to the sub-nanometer level or ideally to one atomic distance. For example, the shear strain should be at least 10,000 and 100,000 for the initial phase sizes of 10 and 100 μm, respectively. Although the phases do not co-deform ideally in real condition of HPT processing,[48)] we introduced shear strains over 10,000 in several Mg-based systems and examined their behaviors.[49–53)]

Both Ti and Zr are totally immiscible in Mg even in the liquid form.[54,55)] However, we detected atomic-scale mixing and the formation of several supersaturated metastable phases in both Mg–Ti[49)] and Mg–Zr[50)] systems after 100–1,000 HPT turns: bcc, fcc and hcp (see Fig. 5 for Mg–Ti). The formation of new phases in the Mg–Ti system was also reported by

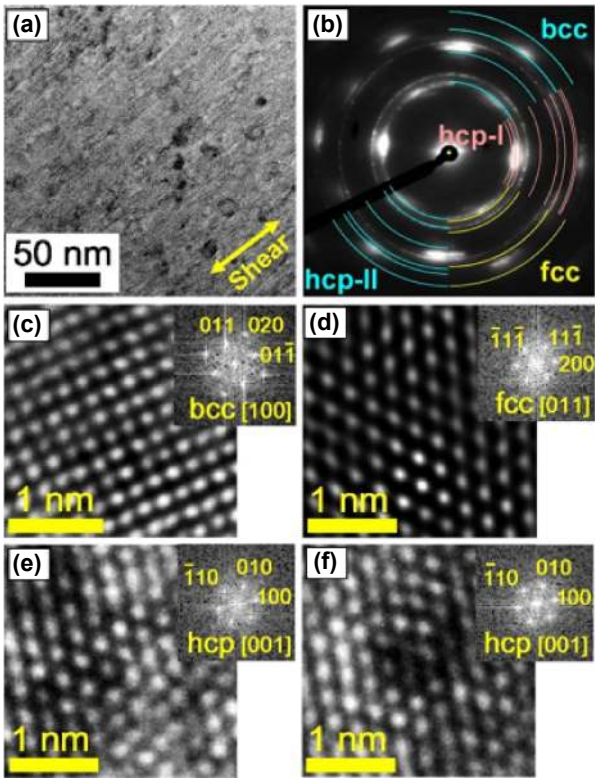


Fig. 5 Formation of bcc, fcc and hcp phases in immiscible Mg–Ti system by ultra-SPD despite full immiscibility of two elements even in liquid form. (a) TEM bright-field image, (b) corresponding SAED pattern and (c–f) TEM lattice images and FFT diffractograms for different phases after HPT processing for 100 turns at room temperature.[48)]

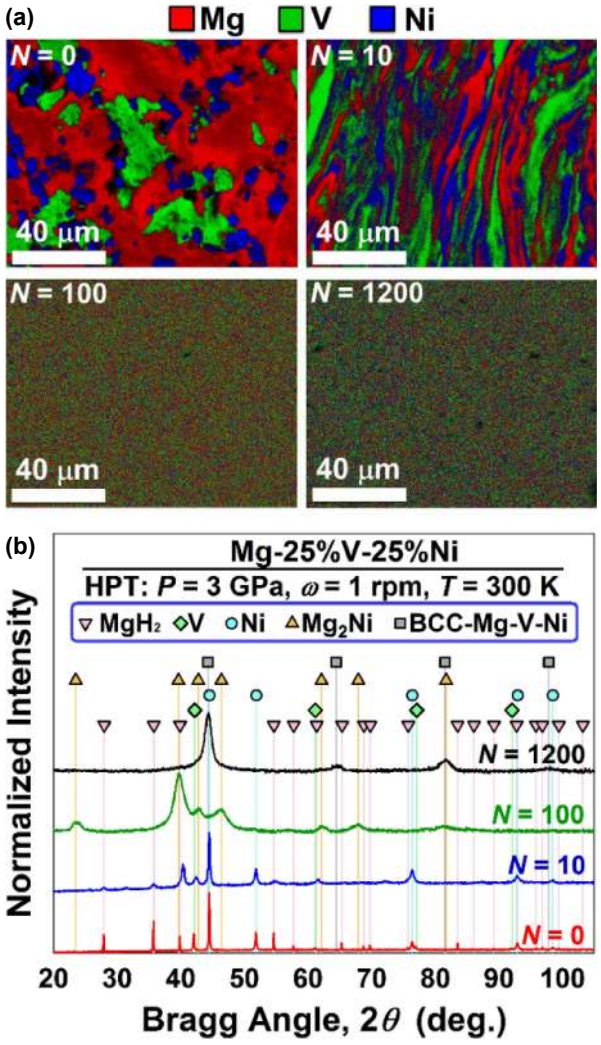


Fig. 6 Elemental mixing in immiscible Mg–V–Ni system and formation of single bcc phase by ultra-SPD. (a) STEM-EDS mapping and (b) XRD profiles after various HPT turns at room temperature.[51)]

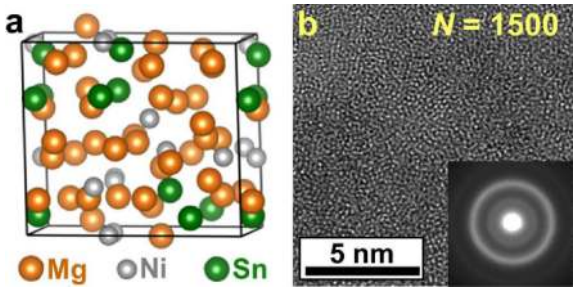


Fig. 7 Amorphization in immiscible Mg–Ni–Sn system by ultra-SPD. (a) Simulated structure by first-principles calculations and (b) TEM lattice image and corresponding SAED pattern after HPT processing for 1,500 turns at room temperature.[51)]

using the high-energy ball milling,[56–58)] but the processing time for ultra-SPD is shorter and the final product has a bulk shape. For the Mg–Zr system, ultra-SPD is currently the only method that provided clear evidence for the presence of new metastable phases in this system.[50)]

The Mg–V- and Mg–Ni-based systems, which are of interest for hydrogen storage, are also immiscible in the wide range of compositions.[43)] We found new bcc phases (sometimes with the B2-type ordering) in the Mg–V,[52)] Mg–V–Sn,[51)] Mg–V–Pd,[51)] Mg–V–Ni,[51)] Mg–V–Cr,[52)] Mg–Ni–Sn[51)] and Mg–Ni–Pd[53)] systems after HPT processing for 1,200–1,500 turns. Figure 6 shows (a) SEM-EDS mapping and (b) XRD profiles for Mg–V–Ni after HPT processing for different turns.[51)] Similar to the Nb–Ti system, the phases were first elongated by shear straining, but they finally mixed at very large strains. While several phases were detected after 100 HPT turns, only a single bcc phase was present after 1,200 turns. In the Mg–Ni–Sn system, elemental mixing was also achieved after 1,500 HPT turns which resulted in the formation of an amorphous phase in good agreement with the prediction of first-principles calculations, as shown in Fig. 7.[51)] In the Mg–Ni–Pd, a single-phase $Mg_4NiPd$ with the bcc structure and CsCl-type (B2) ordering was formed after 1,500 turns.[53)] Detailed analysis by APT, as shown in Fig. 8(a), confirmed that the three elements were mixed at the atomic scale despite their thermodynamic immiscibility.[59)] Moreover, in-situ XRD observations by using a synchrotron facility, as shown in Fig. 8(b), confirmed that the $Mg_4NiPd$ phase was thermally stable up to 400 K.[53)]

Here, it should be noted that various analyses such STEM-EDS, XRD and microstructural examinations confirmed that the structural and microstructural changes occur continuously during ultra-SPD.[50–52)] For example, the changes in EDS mappings and XRD profiles of Figs. 4 and 6 occurs continuously with increasing the number of turns. Two recent studies on the microstructural and structural evolutions during straining in the immiscible Al–Fe[60)] and $MgH_2$–

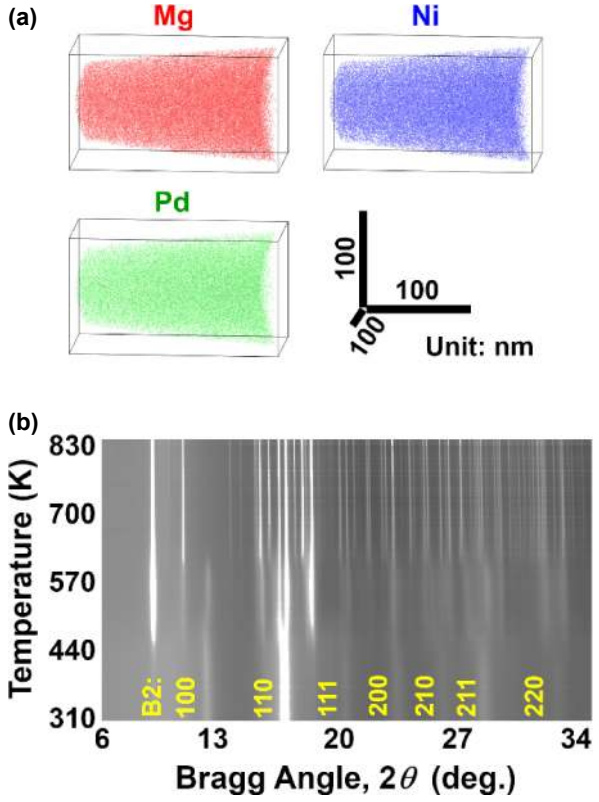


Fig. 8 Atomic-scale mixing of elements and formation of $Mg_4NiPd$ alloy with B2-type structure by ultra-SPD. (a) APT elemental mapping and (b) XRD patterns achieved using synchrotron during heating to examine thermal stability after HPT processing for 1,500 turns at room temperature.[53)]

$TiH_2$[61)] systems also provided clear evidence regarding the continuous characteristic changes during ultra-SPD. Taken altogether, ultra-SPD provides a new pathway to produce new materials, which can be used for different applications, as will be discussed below.

## 3. Properties of Materials Processed by Ultra-SPD

### 3.1 Microhardness evolution

Hardness of metallic materials processed by SPD usually follows three main behaviors with straining.[62,63)] In most of metallic materials with high melting temperatures, hardness increases at the early stages of straining, but it saturates to the steady state at large strains.[63,64)] In materials with moderate melting temperatures such as Al and Mg, the hardness increases with increasing the strain, but after reaching a maximum, decreases and saturates to the steady state.[65,66)] In materials with low melting temperatures, the hardness decreases with straining and saturates to the steady states.[62,67)] In all these materials, the steady states appear at shear strains below 100.[62–67)] However, as shown in Fig. 1, at least for some of materials, the steady-state hardness can change at shear strains over 1,000.[24,25)] In the other word, larger shear strains are required to have a complete balance between the hardening and softening phenomena. These observations suggest that the reported steady states should be considered as "apparent" steady state unless the behavior of materials are examined at larger shear strains.

Another feature that was observed after ultra-SPD is the presence of new hardness-strain behaviors at extremely large strains. As shown in Fig. 9, the Mg–Zr and Mg–Ni–Sn alloys exhibited hardness minimum peaks with straining.[51)] While the Mg–Ni–Pd alloy exhibited an apparent steady-state hardness, no steady-state hardness was detected in the Mg–Zr alloy even by increasing the shear strain to 100,000. It should be noted that the appearance of steady state in the Mg–Ni–Pd alloy does not correspond to the occurence of structural and microstructural steady sates, as clear changes were detected in this material even at shear strains over 10,000.[53)] The Mg–Li alloy exhibited a hardness maximum followed by a softening similar to HPT-processed Al and Mg,[65,66)] but its hardness peak appeared at a large shear strain as 1,000.[53)] Taken altogether, the microhardness measurements confirm that a real steady state in SPD-processed materials is achievable at larger strains than those are currently accepted, especially when the multi-phase materials are processed.

### 3.2 High strength and high plasticity

The materials synthesized by ultra-SPD exhibit quite high hardness levels compared with the as-cast materials due to their nanostructural features.[29–34)] For example, the nano-grained AlNi and TiAl intermetallics synthesized by ultra-SPD exhibited compressive strengths three times higher than the as-cast materials.[29,32)] The $\beta$-Mg alloys, a group of alloys that are under investigation by the group of author using ultra-SPD, exhibited hardness levels in the range of 100–600 Hv, which is comparable with the hardness of $\beta$-Ti biomaterials.[24)] In addition to the high strength, another feature of materials processed by ultra-SPD is their high plasticity under compression. Such a high plasticity was confirmed in the TiAl and $Ni_2AlTi$ intermetallics, which had the microstructural features shown in Figs. 2 and 3, respectively.[32,34)]

Figure 10 shows the results of micropillar compression test conducted on TiAl right after synthesizing by ultra-SPD as well as after post-SPD annealing at 873 K for 24 h. The sample after ultra-SPD exhibited a compressive strength of 2 GPa which is 2 times higher than the earlier reported strength levels for pure TiAl.[68)] After annealing, both strength and plasticity improved due to the activation of different deformation mechanisms such a twinning, dislocation slip and grain boundary sliding.[34)] This promising combination of high strength and high plasticity, which could not be achieved earlier in this system by using other processing routes,[68)] indicates the high potential of ultra-SPD to develop new structural materials.

### 3.3 Room-temperature superplasticity

Superplasticity is defined as the ability of a material to be elongated over 400% under tension.[69)] Superplasticity is an important phenomenon for metal forming, especially when the final products have complicated shapes. Such large elongations are achievable only at homologous temperatures over $0.5T_m$ ($T_m$: melting point) where the grain-boundary sliding is the dominant deformation mechanism in the fine-grained materials.[69)] Although SPD processing showed high potential to achieve low-temperature superplasticity by grain

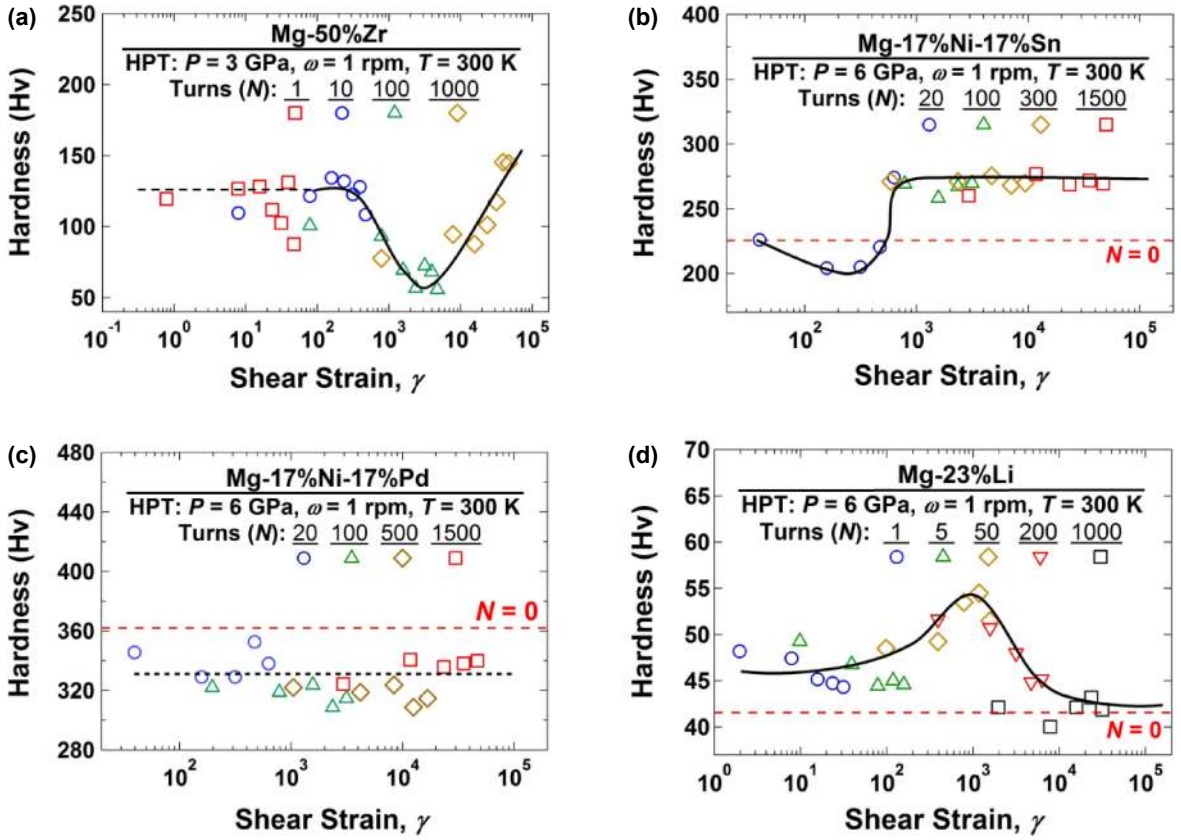


Fig. 9 Unusual hardening/softening behaviors after ultra-SPD. Variations of hardness versus shear strain for (a) Mg–Zr, (b) Mg–Ni–Pd, (c) Mg–Ni–Sn and (d) Mg–Li after HPT processing for various turns.[51)]

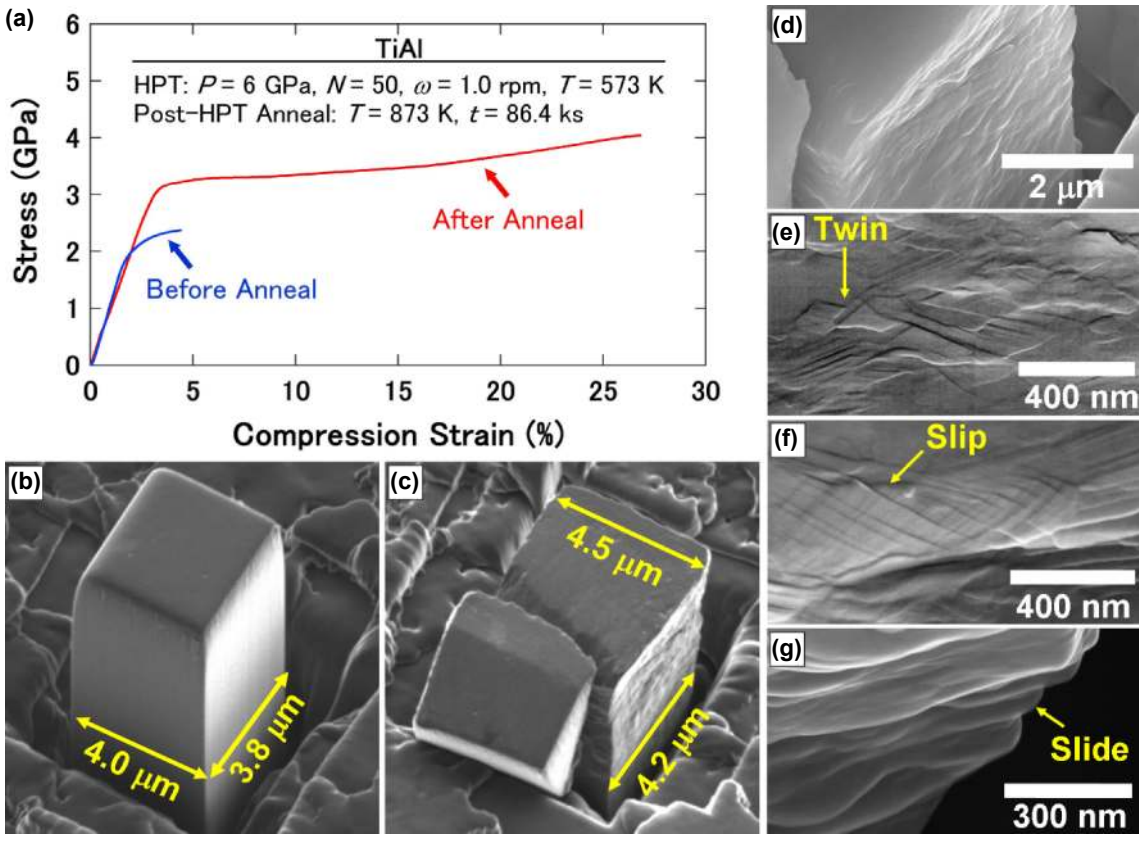


Fig. 10 High strength and high plasticity in TiAl synthesized by ultra-SPD due to activation of different deformation mechanisms under compression. (a) Stress-strain curves achieved by micro-pillar compression test after HPT processing for 50 turns at 673 K and after post-HPT annealing at 873 K for 24 h. Appearance of pillar (b) after post-HPT annealing and before compression and (c–g) after compression.[32)]

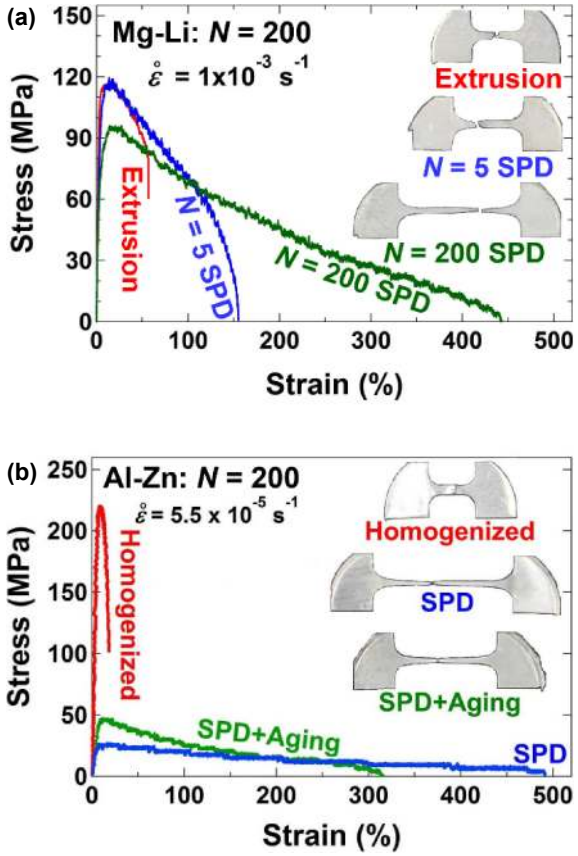


Fig. 11 Occurrence of room-temperature superplasticity in magnesium and aluminum alloys after ultra-SPD. (a) Stress-strain curves for Mg - 8 wt.% Li alloy after extrusion and after HPT processing for 5 and 200 turns at room temperature.[74] (b) Stress-strain curves for Al - 30 at% Zn alloy after homogenization, after HPT processing for 200 turns at room temperature and after post-HPT natural aging at room temperature for 100 days.[75] Inset: appearance of tensile specimens after pulling to failure.

refinement effect,[70–72] there have been few successful attempts to reduce the superplastic deformation temperature below $0.5T_m$.[73] We showed recently that ultra-SPD can be employed to design new superplastic materials by engineering the chemistry and diffusivity of grain boundaries.[74,75]

The application of ultra-SPD by 200 HPT turns to Mg–Li and Al–Zn alloys resulted in increasing the fraction of Mg/Li and Al/Zn interphase boundaries with high grain boundary diffusion and mobility.[74,75] Moreover, Ultra-SPD enhanced the segregation of Li and Zn in the Mg/Mg and Al/Al grain boundaries, respectively.[74,75] Such microstructural modifications resulted in achieving room-temperature superplasticity in the Mg–Li and Al–Zn alloys, as shown in Figs. 11(a) and (b), respectively. These superplastic behaviors, which occurred at $0.35–0.36T_m$, are considered as the first reports on achieving room-temperature superplasticity in any Mg- and Al-based alloys. It should be noted that the application of ultra-SPD was essential to achieve room-temperature superplasticity as earlier attempts using the conventional SPD processing could not lead to room-temperatures superplasticity in the Mg–Li[76–78] and Al–Zn[79,80] alloys. The Mg–Li and Al–Zn processed by ultra-SPD are not so stable at room temperature and they exhibit grain coarsening and unusual hardening during time due to the weakening of grain-boundary sliding.[81]

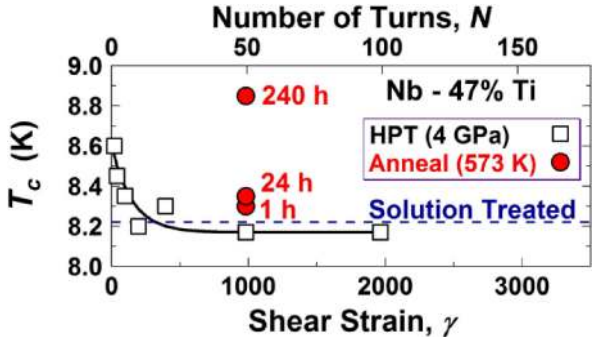


Fig. 12 Synthesis of Nb–Ti superconductors by ultra-SPD. Variations of superconducting critical temperature versus shear strain after HPT processing for various turns at room temperature and after post-HPT annealing at 573 K for different periods of time.[46]

### 3.4 Superconductivity

Superconductivity is the drop of electrical resistivity to zero which occurs below a critical temperature in some particular materials.[82] The Nb–Ti alloys, containing small particles of Ti in Nb matrix, are widely used as superconductor wires in industry.[83,84] These wires are fabricated by repeated cold working and annealing for many times to have a desirable distribution of Ti in Nb.[83,84] We found that the Nb–Ti superconductors can be fabricated directly from the Nb and Ti powders by application of ultra-SPD.[46] As shown in Fig. 12, the transition temperature could be simply adjusted by controlling the shear strain or by adjusting the post-deformation annealing time.[46] The changes in the transition temperature was due to the effect of strain on distribution of Ti in Nb, as shown earlier in Fig. 4. Even at very large strains, the Ti nano-clusters remained in the Nb matrix (Fig. 4(c)) which resulted in good superconducting properties compared with the commercial wires.[83,84] It should be noted although lattice defects generated by SPD processing diminish the electrical conductivity of Cu[85,86] or Cu–Cr conductors,[87,88] they can act as positive features for superconductivity due to their vortex pinning effect.[89] Taken altogether, ultra-SPD is considered as a simple route for fabrication of advanced superconductors, which can be used in micro-devices for electronic applications.

### 3.5 Hydrogen storage

Solid-state hydrogen in the form of metal hydrides or complex hydrides is considered as the most compact technique to store hydrogen fuel under low pressure.[90,91] However, there are several issues that should be addressed for application of these hydrogen storage materials: enhancement of activation, acceleration of hydrogen storage kinetics and reduction of hydrogen desorption temperature.[82,91] It was shown earlier that the application of SPD methods to the hydrogen storage materials can ease the activation (e.g., in TiFe intermetallics[92]) and enhance the hydrogen storage kinetics (e.g., in pure Mg[93,94] and Mg-based alloys[95–97]). Our group first used ultra-SPD to synthesize well-known hydrogen storage materials such as Mg-based binary intermetallics[37] and Ti–V alloys.[47] We later challenged to produce new hydrogen storage materials from different systems such as Mg–Ti as in Fig. 5,[49,61] Mg–Zr,[50] Mg–

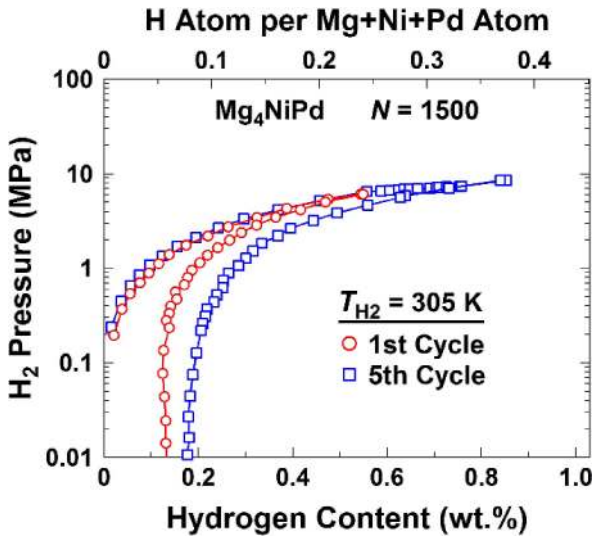


Fig. 13 Reversible room-temperature hydrogen storage in magnesium alloy synthesized by ultra-SPD. Hydrogen pressure-composition isotherms at 305 K for first and fifth hydrogenation/dehydrogenation cycles for $Mg_4NiPd$ produced by HPT processing for 1,500 turns at room temperature.[53)]

V,[52)] Mg–V–Cr alloys,[52)] Mg–V–Ni as in Fig. 6,[51)] Mg–Ni–Sn as in Fig. 7[51)] and Mg–Ni–Pd as in Fig. 8.[53)]

Among the hydrogen storage materials mentioned above, a $Mg_4NiPd$ alloy with the B2-type structure was designed by using first-principle calculations to have low hydrogen binding energy.[53)] Because of the immiscibility of the alloy, ultra-SPD was employed to mix the elements and synthesize a B2-type crystal structure, as shown in Fig. 8. The alloy could reversibly absorb and desorb the hydrogen at room temperature, as shown in Fig. 13.[53)] Although the hydrogen storage capacity of this alloy was rather low, the alloy is considered as the first Mg-based alloy that could reversibly store hydrogen at room temperature. It should be noted that the Mg-based alloys are the first materials introduced as the hydrogen storage materials,[98)] but long-time attempts to reduce their working temperature to room temperature (without addition of rare-earth elements) has not been successful.[90)] The current findings introduce ultra-SPD as a new mechanochemical route to synthesize new hydrogen storage materials at the laboratory scale.[99)]

## 4. Conclusions

The behavior of materials at ultrahigh shear strains over 1,000 (i.e. after ultra-SPD) can be different from their behavior after conventional SPD processing. This difference is especially significant, when the multi-phase materials are processed. Processing of materials by ultra-SPD, which is technically possible using the HPT method, not only provides new insights into the behavior of materials at large shear strains, but also provides a new metallurgical alchemy route to synthesize advanced materials with exceptional structural and functional properties. Despite the potential of the method as a unique processing tool, there are still open questions regarding the mechanism of structural and microstructural evolutions during ultra-SPD as well as the required strain to achieve a real saturation of microstructural features. Moreover, the introduction of ultra-SPD to materials is currently limited to the HPT method, which provides samples with small sizes. New technologies should be developed to impart ultra-SPD in large samples for industrial applications.

## Acknowledgments

The author acknowledges the MEXT, Japan for a Grant-in-Aid for Scientific Research on Innovative Areas (No. 19H05176).

## REFERENCES

1) R.Z. Valiev, R.K. Islamgaliev and I.V. Alexandrov: Prog. Mater. Sci. **45** (2000) 103–189.
2) R.Z. Valiev, Y. Estrin, Z. Horita, T.G. Langdon, M.J. Zehetbauer and Y.T. Zhu: JOM **58**(4) (2006) 33–39.
3) V. Segal: Materials **11** (2018) 1175.
4) A. Azushima, R. Kopp, A. Korhonen, D.Y. Yang, F. Micari, G.D. Lahoti, P. Groche, J. Yanagimoto, N. Tsuji, A. Rosochowski and A. Yanagida: CRIP Ann. **57** (2008) 716–735.
5) M. Zehetbauer, R. Grossinger, H. Krenn, M. Krystian, R. Pippan, P. Rogl, T. Waitz and R. Wurschum: Adv. Eng. Mater. **12** (2010) 692–700.
6) Y. Estrin and A. Vinogradov: Acta Mater. **61** (2013) 782–817.
7) V.I. Levitas, Y. Ma, E. Selvi, J. Wu and J. Patten: Phys. Rev. B **85** (2012) 054114.
8) R.B. Figueiredo, F.L. Sicupira, L. Raquel, C. Malheiros, M. Kawasaki, D.B. Santos and T.G. Langdon: Mater. Sci. Eng. A **625** (2015) 114–118.
9) A.R. Kilmametov, Y. Ivanisenko, A.A. Mazilkin, B.B. Straumal, A.S. Gornakova, O.B. Fabrichnaya, M.J. Kriegel, D. Rafaja and H. Hahn: Acta Mater. **144** (2018) 337–351.
10) A. Bachmaier, M. Kerber, D. Setman and R. Pippan: Acta Mater. **60** (2012) 860–871.
11) M. Kawasaki, B. Ahn, H.J. Lee, A.P. Zhilyaev and T.G. Langdon: J. Mater. Res. **31** (2016) 88–99.
12) K.S. Kormout, R. Pippan and A. Bachmaier: Adv. Eng. Mater. **19** (2017) 1600675.
13) N. Ibrahim, M. Peterlechner, F. Emeis, M. Wegner, S.V. Divinski and G. Wilde: Mater. Sci. Eng. A **685** (2017) 19–30.
14) P.W. Bridgman: Phys. Rev. **48** (1935) 825–847.
15) P.W. Bridgman: J. Appl. Phys. **8** (1937) 328–336.
16) R. Pippan, S. Scheriau, A. Taylor, M. Hafok, A. Hohenwarter and A. Bachmaier: Annu. Rev. Mater. Res. **40** (2010) 319–343.
17) F.A. Mohamed and S.S. Dheda: Mater. Sci. Eng. A **558** (2012) 59–63.
18) M.J. Starink, X.C. Cheng and S. Yang: Acta Mater. **61** (2013) 183–192.
19) V.V. Popov, A.V. Stolbovsky and E.N. Popova: Phys. Met. Metallogr. **118** (2017) 1073–1080.
20) A.P. Zhilyaev and T.G. Langdon: Prog. Mater. Sci. **53** (2008) 893–979.
21) K. Edalati and Z. Horita: Mater. Sci. Eng. A **652** (2016) 325–352.
22) T. Sakai, A. Belyakov, R. Kaibyshev, H. Miura and J.J. Jonas: Prog. Mater. Sci. **60** (2014) 130–207.
23) A. Mishra, B.K. Kad, F. Gregori and M.A. Meyers: Acta Mater. **55** (2007) 13–28.
24) K. Edalati: Unpublished Work.
25) K. Edalati, Z. Horita, H. Fujiwara and K. Ameyama: Metall. Mater. Trans. A **41** (2010) 3308–3317.
26) A. Hosokawa, S. Ii and K. Tsuchiya: Mater. Trans. **55** (2014) 1097–1103.
27) Z. Lee, F. Zhou, R.Z. Valiev, E.J. Lavernia and S.R. Nutt: Scr. Mater. **51** (2004) 209–214.
28) E.Y. Yoon, D.J. Lee, D.H. Ahn, E.S. Lee and H.S. Kim: J. Mater. Sci. **47** (2012) 7770–7776.
29) K. Edalati, S. Toh, M. Watanabe and Z. Horita: Scr. Mater. **66** (2012) 386–389.
30) A. Alhamidi, K. Edalati and Z. Horita: Mater. Sci. Forum **765** (2013) 378–382.

31) A. Alhamidi, K. Edalati, H. Iwaoka and Z. Horita: Philos. Mag. **94** (2014) 876–887.
32) K. Edalati, S. Toh, H. Iwaoka, M. Watanabe, Z. Horita, D. Kashioka, K. Kishida and H. Inui: Scr. Mater. **67** (2012) 814–817.
33) K. Edalati and Z. Horita: Mater. Sci. Forum **765** (2013) 558–562.
34) K. Edalati, T. Daio, Z. Horita, K. Kishida and H. Inui: J. Alloys Compd. **563** (2013) 221–228.
35) K. Oh-ishi, K. Edalati, H.S. Kim, K. Hono and Z. Horita: Acta Mater. **61** (2013) 3482–3489.
36) S. Lee, K. Edalati, H. Iwaoka, Z. Horita, T. Ohtsuki, T. Ohkochi, M. Kotsugi, T. Kojima, M. Mizuguchi and K. Takanashi: Philos. Mag. Lett. **94** (2014) 639–646.
37) H. Emami, K. Edalati, A. Staykov, T. Hongo, H. Iwaoka, Z. Horita and E. Akiba: RSC Adv. **6** (2016) 11665–11674.
38) H. Mehrer: *Numerical Data and Functional Relationships in Science and Technology, Volume 26: Diffusion in Solid Metals and Alloys*, (Springer-Verlag, Berlin, 1990).
39) J.F. Albertsen, J.M. Knudsen and G.B. Jensen: Nature **273** (1978) 453–454.
40) B. Oberdorfer, B. Lorenzoni, K. Unger, W. Sprengel, M. Zehetbauer, R. Pippan and R. Wurschum: Scr. Mater. **63** (2010) 452–455.
41) M. Krystian, D. Setman, B. Mingler, G. Krexner and M.J. Zehetbauer: Scr. Mater. **62** (2010) 49–52.
42) J. Cızek, M. Janecek, O. Srba, R. Kuzel, Z. Barnovska, I. Prochazka and S. Dobatkin: Acta Mater. **59** (2011) 2322–2329.
43) H. Okamoto, M.E. Schlesinger and E.M. Mueller: *ASM Handbook, Volume 3: Alloy Phase Diagrams*, (ASM International, Ohio, 2016).
44) E. Ma: J. Rheol. **50** (2005) 413–509.
45) B.S. Murty and S. Ranganathan: Int. Mater. Rev. **43** (1998) 101–141.
46) K. Edalati, T. Daio, S. Lee, Z. Horita, T. Nishizaki, T. Akune, T. Nojima and T. Sasaki: Acta Mater. **80** (2014) 149–158.
47) K. Edalati, H. Shao, H. Emami, H. Iwaoka, Z. Horita and E. Akiba: Int. J. Hydrogen Energy **41** (2016) 8917–8924.
48) K. Edalati, H. Emami, A. Staykov, D.J. Smith, E. Akiba and Z. Horita: Acta Mater. **99** (2015) 150–156.
49) A. Bachmaier, J. Schmauch, H. Aboulfadl, A. Verch and C. Motz: Acta Mater. **115** (2016) 333–346.
50) K. Edalati, H. Emami, Y. Ikeda, H. Iwaoka, I. Tanaka, E. Akiba and Z. Horita: Acta Mater. **108** (2016) 293–303.
51) K. Edalati, R. Uehiro, K. Fujiwara, Y. Ikeda, H.W. Li, X. Sauvage, R.Z. Valiev, E. Akiba, I. Tanaka and Z. Horita: Mater. Sci. Eng. A **701** (2017) 158–166.
52) K. Fujiwara, R. Uehiro, K. Edalati, H.W. Li, R. Floriano, E. Akiba and Z. Horita: Mater. Trans. **59** (2018) 741–746.
53) K. Edalati, R. Uehiro, Y. Ikeda, H.W. Li, H. Emami, Y. Filinchuk, M. Arita, X. Sauvage, I. Tanaka, E. Akiba and Z. Horita: Acta Mater. **149** (2018) 88–96.
54) J.L. Murray: Bull. Alloy Phase Diag. **7** (1986) 245–248.
55) H. Okamoto: J. Phase Equilibria Diffus. **28** (2007) 305–306.
56) G. Liang and R. Schulz: J. Mater. Sci. **38** (2003) 1179–1184.
57) K. Asano, H. Enoki and E. Akiba: Mater. Trans. **48** (2007) 121–126.
58) G. Calmak, Z. Karoly, I. Mohai, T. Ozturk and J. Szepvolgyi: Int. J. Hydrogen Energy **35** (2010) 10412–10418.
59) K.P. Gupta: J. Phase Equilibria Diffus. **25** (2004) 191–194.
60) A. Duchaussoy, X. Sauvage, K. Edalati, Z. Horita, G. Renou, A. Deschamps and F. De Geuser: Acta Mater. **167** (2019) 89–102.
61) K. Kitabayashi, K. Edalati, H.W. Li, E. Akiba and Z. Horita: Adv. Eng. Mater. (2019) in press. doi:10.1002/adem.201900027.
62) K. Edalati, J.M. Cubero-Sesin, A. Alhamidi, I.F. Mohamed and Z. Horita: Mater. Sci. Eng. A **613** (2014) 103–110.
63) M. Kawasaki, R.B. Figueiredo, Y. Huang and T.G. Langdon: J. Mater. Sci. **49** (2014) 6586–6596.
64) D.J. Lee, E.Y. Yoon, D.H. Ahn, B.H. Park, H.W. Park, L.J. Park, Y. Estrin and H.S. Kim: Acta Mater. **76** (2014) 281–293.
65) M. Kawasaki, R.B. Figueiredo and T.G. Langdon: Acta Mater. **59** (2011) 308–316.
66) S. Panda, L.S. Toth, J.J. Fundenberger, O. Perroud, J. Guyon, J. Zou and T. Grosdidier: Mater. Charact. **123** (2017) 159–165.
67) B. Srinivasarao, A.P. Zhilyaev, T.G. Langdon and M.T. Perez-Prado: Mater. Sci. Eng. A **562** (2013) 196–202.
68) T.W. Kim, R. Wagner and M. Yamaguchi (Eds.): *Gamma Titanium Aluminides*, (TMS, Warrendale, PA, 1995).
69) T.G. Langdon: J. Mater. Sci. **44** (2009) 5998–6010.
70) R.Z. Valiev, O.A. Kaibyshev, R.I. Kuznetsov, R.S. Musalimov and N.K. Tsenev: Dokl. Akad. Nauk SSSR **301** (1988) 864–866.
71) Y. Ma, M. Furukawa, Z. Horita, M. Nemoto, R.Z. Valiev and T.G. Langdon: Mater. Trans. **37** (1996) 336–339.
72) M. Kawasaki, R.B. Figueiredo, C. Xu and T.G. Langdon: Metall. Mater. Trans. A **38** (2007) 1891–1898.
73) S.X. McFadden, R.S. Mishra, R.Z. Valiev, A.P. Zhilyaev and A.K. Mukherjee: Nature **398** (1999) 684–686.
74) K. Edalati, T. Masuda, M. Arita, M. Furui, X. Sauvage, Z. Horita and R.Z. Valiev: Sci. Rep. **7** (2017) 2662.
75) K. Edalati, Z. Horita and R.Z. Valiev: Sci. Rep. **8** (2018) 6740.
76) P. Metenier, G. Gonzalez-Doncel, O.A. Ruano, J. Wolfenstine and O.D. Sherby: Mater. Sci. Eng. A **125** (1990) 195–202.
77) M. Furui, C. Xu, T. Aida, M. Inoue, H. Anada and T.G. Langdon: Mater. Sci. Eng. A **410–411** (2005) 439–442.
78) H. Matsunoshita, K. Edalati, M. Furui and Z. Horita: Mater. Sci. Eng. A **640** (2015) 443–448.
79) R.Z. Valiev, M.Y. Murashkin, A. Kilmametov, B. Straumal, N. Chinh and T.G. Langdon: J. Mater. Sci. **45** (2010) 4718–4724.
80) A. Alhamidi, K. Edalati, Z. Horita, S. Hirosawa, K. Matsuda and D. Terada: Mater. Sci. Eng. A **610** (2014) 17–27.
81) K. Edalati, Y. Hashiguchi, H. Iwaoka, H. Matsunaga, R.Z. Valiev and Z. Horita: Mater. Sci. Eng. A **729** (2018) 340–348.
82) C.P. Poole, Jr., H.A. Farach, R.J. Creswick and R. Prozorov: *Superconductivity*, Second Edition, (Elsevier, Amsterdam, 2007).
83) C. Meingast and D.C. Larbalestier: J. Appl. Phys. **66** (1989) 5971–5983.
84) L.D. Cooley, P.D. Jablonski, P.J. Lee and D.C. Larbalestier: Appl. Phys. Lett. **58** (1991) 2984–2986.
85) S.A. Hosseini and H. Danesh-Manesh: Mater. Des. **30** (2009) 2911–2918.
86) K. Edalati, K. Imamura, T. Kiss and Z. Horita: Mater. Trans. **53** (2012) 123–127.
87) K.X. Wei, W. Wei, F. Wang, Q.B. Du, I.V. Alexandrov and J. Hu: Mater. Sci. Eng. A **528** (2011) 1478–1484.
88) S.V. Dobatkin, J. Gubicza, D.V. Shangina, N.R. Bochvar and N.Y. Tabachkova: Mater. Lett. **153** (2015) 5–9.
89) V.A. Beloshenko and V.V. Chishko: Phys. Met. Metallogr. **114** (2013) 992–1002.
90) M. Dornheim, S. Doppiu, G. Barkhordarian, U. Boesenberg, T. Klassen, O. Gutfleisch and R. Bormann: Scr. Mater. **56** (2007) 841–846.
91) S. Orimo, Y. Nakamori, J.R. Eliseo, A. Zuttel and C.M. Jensen: Chem. Rev. **107** (2007) 4111–4132.
92) K. Edalati, J. Matsuda, A. Yanagida, E. Akiba and Z. Horita: Int. J. Hydrogen Energy **39** (2014) 15589–15594.
93) D.R. Leiva, A.M. Jorge, T.T. Ishikawa, J. Huot, D. Fruchart, S. Miraglia, C.S. Kiminami and W.J. Botta: Adv. Eng. Mater. **12** (2010) 786–792.
94) T. Grosdidier, J.J. Fundenberger, J.X. Zou, Y.C. Pan and X.Q. Zeng: Int. J. Hydrogen Energy **40** (2015) 16985–16991.
95) A. Revesz, Z. Kanya, T. Verebelyi, P.J. Szabo, A.P. Zhilyaev and T. Spassov: J. Alloys Compd. **504** (2010) 83–88.
96) V.M. Skripnyuk, E. Rabkin, Y. Estrin and R. Lapovok: Acta Mater. **52** (2004) 405–414.
97) M. Krystian, M.J. Zehetbauer, H. Kropik, B. Mingler and G. Krexner: J. Alloys Compd. **509** (2011) S449–S455.
98) E. Wiberg, H. Goeltzer and R. Bauer: Z. Naturforsch. B **6** (1951) 394–395.
99) J. Huot, D.B. Ravnsbæk, J. Zhang, F. Cuevas, M. Latroche and T.R. Jensen: Prog. Mater. Sci. **58** (2013) 30–75.